Energetics of Concerted Two-Electron Transfer and Metal−Metal Bond Cleavage in Phosphido-Bridged Molybdenum and Tungsten Carbonyl Complexes

Darrell Uhrhammer and Franklin A. Schultz*

Department of Chemistry, Indiana University Purdue University Indianapolis, 402 North Blackford Street, Indianapolis, Indiana 46202-3274

Received: July 8, 2002; In Final Form: August 29, 2002

The kinetics and thermodynamics of concerted two-electron transfer and metal−metal bond cleavage in the binuclear phosphido-bridged complexes $[M_2(\mu\text{-}PPh_2)_2(CO)_8]^{0/2-}$ [M = Mo (**1**$^{0/2-}$), W(**2**$^{0/2-}$)] have been determined by variable scan-rate cyclic voltammetry in 0.3 M $TBAPF_6$/acetone. The reductions of **1**° and **2**° are accompanied by an increase of 1.08 Å in M−M distance and expansion and contraction by 29° of the M−P−M and P−M−P angles, respectively, within an intact $M_2(\mu\text{-}PPh_2)_2$ unit. The one-electron electrode potentials of these systems are highly inverted: $\Delta E^{\circ\prime} = E_2^{\circ\prime} - E_1^{\circ\prime} = +0.17$ V for **1**$^{0/2-}$ and +0.18 V for **2**$^{0/2-}$, and the rate constant of the second heterogeneous electron-transfer reaction is smaller than the first: $k_{sh,2}/k_{sh,1} = 0.1$ for Mo and 0.018 for W. Results are consistent with progressive cleavage of the metal−metal bond in two one-electron steps, of which the second is rate-limiting, because it is accompanied by a larger part of the structural change. EHMO calculations reveal that the redox-active orbital is a metal−metal antibonding (σ^*) orbital with substantial bridging-ligand character that decreases markedly in energy on passing from the metal−metal bonded $M(I)_2$ state to nonbonded $M(0)_2$. Despite this feature, electron-transfer thermodynamics and kinetics are not significantly metal-dependent. Rather, comparisons with structurally similar sulfido-bridged complexes reveal that electron-transfer energetics are influenced more extensively by the bridging ligand, with more positive potentials and larger electron-transfer rates observed for RS^- versus R_2P^- bridged species.

Introduction

Concerted multielectron transfer reactions occur widely in chemistry and biology.[1−4] Although seemingly paradoxical, the electrostatic restrictions on such processes are lifted when an accompanying structural or compositional change (proton transfer,[5] ligand binding,[6] or ion-pair formation[7]) makes transfer of a second unit of charge more favorable than the first. Some years ago, we encountered a family of ligand-bridged binuclear complexes that undergo one-step, two-electron transfer by a mechanism wherein the stoichiometry of the redox center does not change.[8−11] Experimental[8−15] and computational[16−22] studies have been conducted on many such systems, from which it is evident that metal−metal bond cleavage accompanied by structural reorganization provides the necessary driving force for a multielectron event.

Concerted multiple electron transfer and metal−metal bond cleavage within a compositionally invariant redox center has relevance to biological processes including nitrogen fixation.[23] The site of this important biological transfomation is thought to be the polynuclear ($MoFe_7S_9$) iron−molybdenum cofactor (FeMoco) within the MoFe protein of nitrogenase. The intermetal distances found in the semi-reduced state of FeMoco[24] are consistent with metal−metal bonding but are too short to permit binding of substrate N_2. It has been suggested[25] that electron transfer accompanied by metal−metal bond cleavage could loosen the Mo−Fe−S framework of FeMoco to provide access to substrate binding as the enzyme is reduced to its catalytically competent level. Several pieces of evidence support this possibility. Coucouvanis and co-workers[26,27] have prepared a polynuclear Mo−Fe−S cluster in which an increase by two in the valence electron count of the molecule results in a lengthening of one Fe−Fe bond by 1.0 Å. Recent electrochemical studies of FeMoco extracted from the MoFe protein of nitrogenase reveal that a one-step, two-electron reduction of the cofactor can be achieved at negative potential under an atmosphere of CO.[28] Finally, the Fe_8S_7 P-cluster in the MoFe protein of nitrogenase[29] and the Fe_4S_4 center in its conjugate Fe protein,[30] which supply electrons in a serial manner to FeMoco, each has been shown to exhibit two-electron redox behavior.

CHART 1

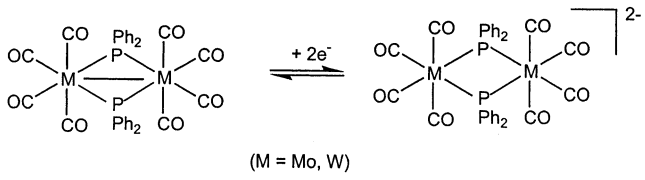

In this paper, we report on the electrochemical kinetics and thermodynamics of coupled two-electron transfer and metal−metal bond cleavage in the binuclear phosphido-bridged complexes $[M_2(\mu\text{-}PPh_2)_2(CO)_8]^{0/2-}$ (M = Mo, **1**$^{0/2-}$; M = W, **2**$^{0/2-}$; Chart 1).[31−33] These reactions occur by sequential one-electron steps

$$[M_2(\mu\text{-}PPh_2)_2(CO)_8] + e^- \rightleftharpoons [M_2(\mu\text{-}PPh_2)_2(CO)_8]^- \quad (E_1^{\circ\prime}, \alpha_1, k_{sh,1}) \quad (1)$$

$$[M_2(\mu\text{-}PPh_2)_2(CO)_8]^- + e^- \rightleftharpoons [M_2(\mu\text{-}PPh_2)_2(CO)_8]^{2-} \quad (E_2^{\circ\prime}, \alpha_2, k_{sh,2}) \quad (2)$$

* Address correspondence to this author. Telephone: (317) 278-2027. Fax: (317) 274-4701. E-mail: schultz@chem.iupui.edu.

10.1021/jp021557z CCC: $22.00 © 2002 American Chemical Society
Published on Web 11/06/2002

of which the second is thermodynamically more favorable than the first ($E_1^{\circ\prime} < E_2^{\circ\prime}$). This inverted potential behavior[34,35] results from the structural changes that accompany reduction of the metal−metal bonded $M(I)_2$ center to nonbonded $M(0)_2$. During this process, the M−M distance increases by 1.08 Å and the M−P−M and P−M−P bridge angles expand and contract, respectively, by ∼29° as the $M_2(\mu\text{-}PPh_2)_2$ unit remains intact.[31−33]

The phosphido-bridged complexes in Chart 1 are selected for study for two reasons. One is that they are experimentally more tractable than the corresponding sulfido-bridged complexes, which are susceptible to CO loss by solvolysis in the $M(I)_2$ oxidation state.[9] A second reason is that it has not been possible to determine accurate values for the kinetic and thermodynamic parameters of reactions 1 and 2 for the RS^- bridged complexes, because the electron-transfer kinetics of these systems are quite fast.[10] Study of $\mathbf{1}^{0/2-}$ and $\mathbf{2}^{0/2-}$ was undertaken in the hope that the phosphido-bridged couples might exhibit more sluggish charge-transfer kinetics, which would permit a mechanistic analysis of multielectron behavior. This paper presents the results of such an investigation and an interpretation of the influence of metal atom and bridging ligand on the concerted two-electron transfer and metal−metal bond cleavage exhibited by these compounds.

Experimental Section

Materials. The complexes $Mo_2(\mu\text{-}PPh_2)_2(CO)_8$ and $W_2(\mu\text{-}PPh_2)_2(CO)_8$ were prepared following the procedures in ref 31 and characterized by UV-visible and infrared spectroscopy. The $M(CO)_5(PPh_2H)$ (M = Mo, W) starting materials were prepared as described in ref 36. Reagents and solvents were obtained commercially in the purest form available and used as received. Synthetic operations were carried out on a Schlenk line under an atmosphere of nitrogen.

Electrochemical measurements were carried out in acetone containing 0.3 M tetra-*n*-butylammonium hexafluorophosphate ($TBAPF_6$) supporting electrolyte. Acetone was obtained as "B & J Brand" solvent from VWR Scientific Products and put through several freeze-pump-thaw cycles and purged with Ar before use. $TBAPF_6$ was used as received from Southwestern Analytical Chemicals or obtained from GFS Chemicals and recrystallized from ethanol−water and dried in vacuo at 100 °C.

Electrochemical Measurements. Electrochemical measurements were conducted in a three-electrode cell containing a Bioanalytical Systems (BAS) mercury drop (CGME) working electrode having an area of 1.16×10^{-2} cm^2, a BAS Ag/AgCl (3M NaCl) reference electrode, and a Pt wire auxiliary electrode. Cyclic voltammetry experiments at scan rates, υ, of 0.01−50 V s^{-1} were conducted with a BAS CV-50W potentiostat. Experiments at $\upsilon \geq 10$ V s^{-1} were conducted with the laboratory-built three-electrode potentiostat described in ref 37 and employed an EG&G PAR 175 waveform generator. Experimental traces were captured on a Nicolet 4094C digital oscilloscope, transferred to a personal computer, and analyzed using a modified version of the Nicolet file transfer software (Henry, version 1.2). A diffusion coefficient of $D = 1.3 \times 10^{-5}$ cm^2 s^{-1} was determined for $Mo_2(\mu\text{-}PPh_2)_2(CO)_8$ in 0.3 M $TBAPF_6$/acetone by chronocoulometry. Other species were assumed to have the same value of D.

Electrochemical kinetic parameters were determined from scan-rate dependent cyclic voltammetric data. Electronic compensation of solution resistance, R_u, was not employed. Rather, reactant concentrations and sweep rates were selected to limit R_u to acceptably small values, and the existing resistance was included in digital simulations. Uncompensated solution resistance was calculated from the equation, $R_u = \rho/4\pi r_o$,[38] where r_o is the electrode radius (0.0314 cm) and ρ is the resistivity of the solvent and supporting electrolyte. The resistivity of 0.3 M $TBAPF_6$/acetone was measured with a Yellow Springs Instrument resistance bridge and a Model 3401 dip-type cell and found to equal 66 Ω cm, from which $R_u = 168$ Ω. Quantitative analysis of electrode kinetic data was limited to results obtained at $0.5 \leq \upsilon \leq 100$ V s^{-1} and C ≤ 0.3 mM. Under these conditions, the largest uncompensated iR_u drop encountered was 10 mV. The lower limit of υ was adopted because the electrochemical response at smaller values was too reversible to yield useful kinetic information. The double-layer capacitance in 0.3 M $TBAPF_6$/acetone was measured as $C_{dl} = i/\upsilon$ from background scans by cyclic voltammetry and found to equal 6.2×10^{-8} F.

Final values of electrode kinetic parameters were obtained by fitting simulated voltammograms to experimental ones using Digisim 2.1 or 3.0 (BAS).[39] Initial estimates of $E_1^{\circ\prime}$, $k_{sh,1}$, α_1, $E_2^{\circ\prime}$, $k_{sh,2}$, and α_2, determined as described in the Results section, and experimental values of $R_u = 168$ Ω, $C_{dl} = 6.2 \times 10^{-8}$ F, $D = 1.3 \times 10^{-5}$ cm^2 s^{-1}, Hg drop mass = 1.63 mg, and $C = 0.1-0.3$ mM were used as input parameters for simulations employing spherical electrode geometry and Butler−Volmer kinetics. Simulated voltammograms were fit to experimental traces at four sweep rates between 10 and 100 V s^{-1} for each couple. The simulations were initiated using $\Delta E^{\circ\prime} = E_2^{\circ\prime} - E_1^{\circ\prime}$ as the varied parameter. After a fit was obtained, $k_{sh,2}$ was allowed to vary and the process was repeated; $k_{sh,1}$ was fit after every third cycle. Final values were taken when the first three significant figures of the varied parameters did not change over three cycles.

EHMO Calculations. Extended Hückel molecular orbital calculations of the H_2P^- bridged analogues of $\mathbf{1}^{0/2-}$ and $\mathbf{2}^{0/2-}$ were carried out on a Gateway 2000 personal computer using the CACAO program.[40] Bond distances and bond angles were obtained from X-ray structural data of $[Mo_2(\mu\text{-}PPh_2)_2(CO)_8]$,[33] $[Li(THF)_3]_2[Mo_2(\mu\text{-}PPh_2)_2(CO)_8]$,[32] $[W_2(\mu\text{-}PPh_2)_2(CO)_8]$,[31] and $[Li(THF)_3]_2[W_2(\mu\text{-}PPh_2)_2(CO)_8]$.[31] A value of 1.47 Å was assumed for the P−H distance. Structures were confined to idealized D_{2h} symmetry. Eight intermediate structures were calculated using a C program on an SGI computer by taking the coordinates of the atoms in the neutral molecules and changing them in a stepwise fashion to the atomic coordinates in the dianions. EHMO calculations were performed on the 10 structures, and the energies of the metal atom d orbitals were plotted versus the M−P−M angle to create a Walsh diagram.

Results

Electrochemical Behavior. Figure 1a displays a cyclic voltammogram for the reduction of $Mo_2(\mu\text{-}PPh_2)_2(CO)_8$ at a scan rate of 0.15 V s^{-1}. Single forward and reverse waves are observed that correspond to the reduction of $\mathbf{1}^\circ$ and reoxidation of $\mathbf{1}^{2-}$ by the sum of eqs 1 and 2. The apparent formal potential, $E_{obs}^{\circ\prime} = (E_{pc} + E_{pa})/2$, is −0.917 V. The cathodic peak current parameter, $i_{pc}/\upsilon^{1/2}AC$, equals 1500 μA s$^{1/2}$ V$^{-1/2}$ cm^{-2} mM^{-1} and is consistent with an overall two-electron transfer. Scans recorded over a sweep rate range of 0.01−1000 V s^{-1} reveal only the single reduction and oxidation waves shown in Figure 1, indicating that the one-electron electrode reactions are not resolved under the experimental conditions. The difference between the cathodic and anodic peak potentials, ΔE_p, equals 78 mV at $\upsilon = 0.15$ V s^{-1} and increases to 280 mV at $\upsilon = 100$ V s^{-1} (Figure 1b). Similar behavior is exhibited by $\mathbf{2}^{0/2-}$, for which $E_{obs}^{\circ\prime} = -0.880$ V and ΔE_p increases from 148 mV at $\upsilon = 0.15$ V s^{-1} to 380 mV at $\upsilon = 100$ V s^{-1}. The large scan-rate

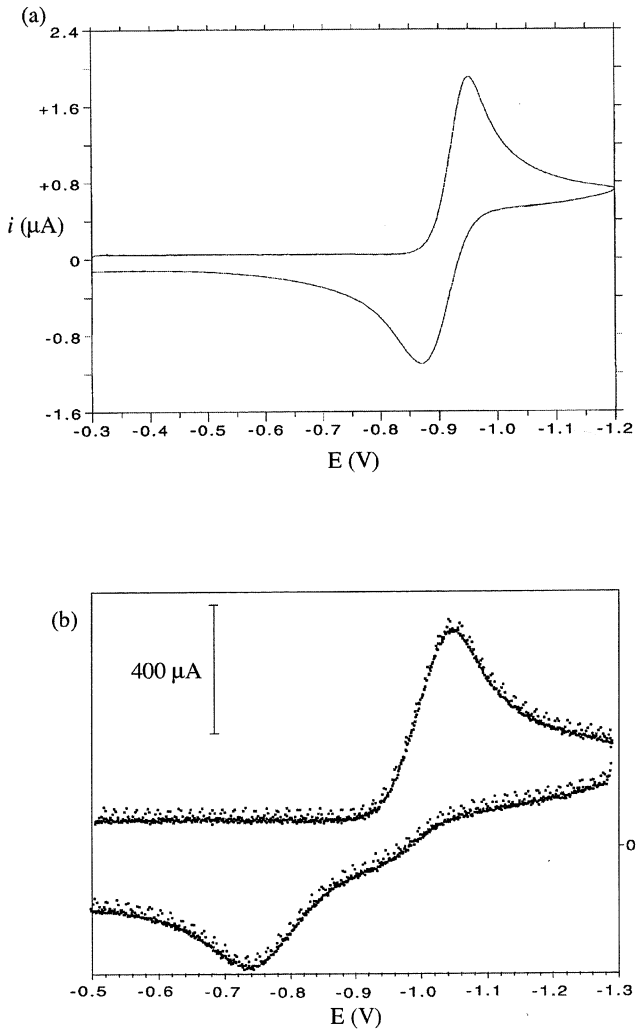

Figure 1. Cyclic voltammograms of 0.28 mM **1**° in 0.3 M $TBAPF_6$/acetone at (a) $v = 0.15$ V s^{-1} and (b) $v = 100$ V s^{-1}.

dependent separation between the cathodic and anodic peak potentials of the $[M_2(\mu\text{-}PPh_2)_2(CO)_8]^{0/2-}$ couples is illustrated in Figure 2.

The kinetic behavior of $\mathbf{1}^{0/2-}$ and $\mathbf{2}^{0/2-}$ contrasts with that of the corresponding sulfido-bridged complexes, $[M_2(\mu\text{-}SR)_2(CO)_8]^{0/2-}$ (M = Mo, W; R = Ph, Bz, *t*-Bu), for which $\Delta E_p \approx 30$ mV at slow-scan rates[9] and increases to 120 mV at $v = 40$ V s^{-1} when M = W and R = Bz ($\mathbf{3}^{0/2-}$).[10] In addition, the RS^- bridged species are reduced at much less negative potentials than their Ph_2P^- bridged counterparts. Electrochemical data for the two families of compounds are compared in Table 1. The thermodynamics of $M(I)_2$ to $M(0)_2$ reduction is influenced dramatically by the donor atom of the bridging ligand but is relatively independent of metal.

Mechanism Analysis. The principal objective of this work is to obtain values for the electrochemical rate constants and formal potentials of eqs 1 and 2. In doing so, it is important to recognize that the existence of potential inversion (defined as $\Delta E^{\circ\prime} = E_2^{\circ\prime} - E_1^{\circ\prime}$) places a "kinetic burden" on the reaction,[35] which causes charge-transfer kinetics to appear more sluggish than they actually are. This interdependence of $\Delta E^{\circ\prime}$ and k_{sh} is resolved by use of the following procedure based on Ryan's analysis of two-electron electrochemical reactions.[41] (1) The rate-limiting electron-transfer step is identified, and its transfer coefficient, α, is evaluated. (2) Initial estimates of $\Delta E^{\circ\prime}$ and the rate-limiting k_{sh} value are obtained by simultaneous solution

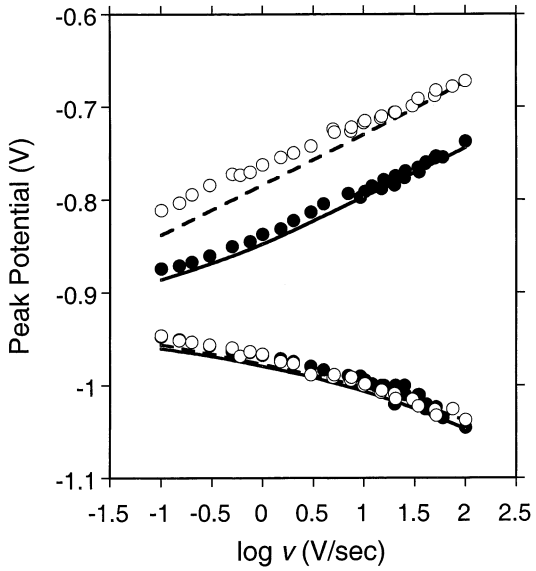

Figure 2. Plots of experimental peak potentials versus log v for $\mathbf{1}^{0/2-}$ (●) and $\mathbf{2}^{0/2-}$ (○). Values of E_{pc} and E_{pa} obtained as a function of scan rate from digital simulations using the parameters in Table 2 are shown as solid and dashed lines for $\mathbf{1}^{0/2-}$ and $\mathbf{2}^{0/2-}$, respectively.

TABLE 1: Electrochemical Data for Two-Electron Redox Couples of Phosphido- and Sulfido-Bridged Complexes

couple	$E_{obs}^{\circ\prime}$ (V)[c]	ΔE_p (mV)[d]	i_{pr}/i_{pf}	$i_p/v^{1/2}AC$[e]
$[Mo_2(\mu\text{-}PPh_2)_2(CO)_8]^{0/2-}$ [a]	−0.92	78	0.80	1500
$[W_2(\mu\text{-}PPh_2)_2(CO)_8]^{0/2-}$ [a]	−0.88	148	0.70	1300
$[Mo_2(\mu\text{-}SPh)_2(CO)_8]^{0/2-}$ [b]	−0.36	25	0.94	1980
$[W_2(\mu\text{-}SPh)_2(CO)_8]^{0/2-}$ [b]	−0.38	25	0.94	1850

[a] Obtained by reduction of neutral forms at 0.15 V s^{-1} in 0.3 M $TBAPF_6$/acetone. [b] Obtained by oxidation of dianion forms at 0.1 V s^{-1} in 0.1 M $TBABF_4/CH_3CN$, from ref 9. [c] $(E_{pc} + E_{pa})/2$. [d] $|E_{pc} - E_{pa}|$. [e] Units of μA $s^{1/2}$ $V^{-1/2}$ cm^{-2} mM^{-1}.

of linear equations derived from the experimental dependence of ΔE_p and the cathodic peak width ($E_{pc} - E_{pc/2}$) on scan rate. (3) The initial estimates are used as input parameters for digital simulations, which are fit to experimental voltammograms to obtain final values of $E_1^{\circ\prime}$, $E_2^{\circ\prime}$, $k_{sh,1}$, and $k_{sh,2}$.

The Rate-Limiting Reaction and Transfer Coefficient. Identification of the rate-limiting step requires that a system be observed under conditions that cause one of the electrode reactions to become noticeably slower than the other. This circumstance is achieved for the phosphido-bridged complexes at $v \geq 0.5$ V s^{-1}, where the anodic peaks of $\mathbf{1}^{0/2-}$ (Figure 1b) and $\mathbf{2}^{0/2-}$ become smaller and broader than their cathodic counterparts. This observation indicates that the second electron transfer (eq 2) is rate-limiting.[41a]

The transfer coefficient of the slow electrode reaction can be evaluated in the following ways. These are based on (i) the relationship between α_2 and the anodic-to-cathodic peak current ratio (eq 3), (ii) the scan-rate dependence of the anodic peak potential (eq 4), and (iii) the width of the anodic peak (eq 5):

$$i_{pa}/i_{pc} = [(1 - \alpha_2)/(1 + \alpha_2)]^{1/2} \quad (3)$$

$$\Delta E_{pa}/\Delta \log v = 0.0295/(1 - \alpha_2) \quad (4)$$

$$E_{pa} - E_{pa/2} = 0.0477/(1 - \alpha_2) \quad (5)$$

For $\mathbf{1}^{0/2-}$, values of $\alpha_2 = 0.38$, 0.39, and 0.38 are obtained by use of eqs 3, 4, and 5, respectively. The mean value of $\alpha_2 = 0.38$ is used as the initial value in the simulations. For $\mathbf{2}^{0/2-}$,

values of $\alpha_2 = 0.29$, 0.43, and 0.34 are obtained by use of eqs 3, 4, and 5, respectively. The value $\alpha_2 = 0.43$ from eq 4 is used in the simulations.

Estimation of $\Delta E^{\circ\prime}$ and $k_{sh,2}$. Because the second electron transfer is the slow step, it is assumed that $k_{sh,1}$ is large and that $\alpha_1 = 0.5$. This assumption is based on the observation that the cathodic peak width is close to the reversible value of 28 mV at low sweep rates. Estimates of $\Delta E^{\circ\prime}$ and $k_{sh,2}$ are obtained from the sweep-rate dependence of two experimentally based parameters. The first quantity is ψ_2', which is a dimensionless electron-transfer rate parameter defined by eq 6:

$$\log \psi_2' = \log k_{sh,2} - \log(\pi FDv/RT)^{1/2} - (1 - \alpha_2)F\Delta E^{\circ\prime}/4.6RT \quad (6)$$

Log ψ_2' is obtained from values of ΔE_p measured as a function of sweep rate by use of eq 7, which is obtained by rearrangement of eq 41 in ref 41a.[42] A plot of experimental values of log ψ_2'

$$\log \psi_2' = (1 - \alpha_2^2)\log(\alpha_2/2\pi)/4(1 + \alpha_2) - (1 - \alpha_2^2)\log[(1 - \alpha_2)/2\pi]/4(1 + \alpha_2) + 0.339 - (1 - \alpha_2^2)\Delta E_p/0.118 \quad (7)$$

versus log v for $\mathbf{1}^{0/2-}$ yields a linear relationship of log $\psi_2' = -0.53 \log v - 1.14$. The slope of the line is in good agreement with the value -0.50 predicted by eq 6. The intercept of the log ψ_2' versus log v plot in conjunction with eq 6 and values of $D = 1.3 \times 10^{-5}$ cm^2 s^{-1} and $\alpha_2 = 0.38$ establishes one linear relationship between $\Delta E^{\circ\prime}$ and $k_{sh,2}$ for the Mo couple.

$$\log(k_{sh,2})_{Mo} = 5.21(\Delta E^{\circ\prime})_{Mo} - 2.54 \quad (8a)$$

A similar approach for $\mathbf{2}^{0/2-}$ produces a linear relationship of log $\psi_2' = -0.54 \log v - 1.62$, which in conjunction with eq 6, $D = 1.3 \times 10^{-5}$ cm^2 s^{-1}, and $\alpha_2 = 0.43$ results in the following relationship for the W couple:

$$\log(k_{sh,2})_W = 4.84(\Delta E^{\circ\prime})_W - 3.03 \quad (8b)$$

The second kinetic parameter, ΔE_{BC}, accounts for the influence of slow electron-transfer kinetics on the observed potential of reduction. ΔE_{BC} is determined from the broadening of the cathodic peak with increasing scan rate under conditions where the first electron transfer exhibits rate-limiting behavior. This occurs at $v \geq 0.5$ V s^{-1}. Values of ΔE_{BC} are obtained from the working curve of ΔE_{BC} versus $E^*_{ppc/2}$ in Figure 5 of ref 41a, where $E^*_{ppc/2} = (E_{pc} - E_{pc/2})/(1 + \alpha_2)$ is the cathodic peak width normalized by $(1 + \alpha_2)$. Equation 9 describes the dependence of ΔE_{BC} on $k_{sh,2}$, $\Delta E^{\circ\prime}$ and other kinetic parameters:

$$\Delta E_{BC} = [0.059 \log k_{sh,2}/(1 + \alpha_2)] - [0.059 \log(\pi FDv/RT)^{1/2}/(1 + \alpha_2)] - [0.059(1 - \alpha_2)F\Delta E^{\circ\prime}/4.6(1 + \alpha_2)RT] + \Delta E^{\circ\prime}/2 \quad (9)$$

A plot of ΔE_{BC} versus log v yields a linear relationship of $\Delta E_{BC} = -0.021 \log v + 0.0320$ for $\mathbf{1}^{0/2-}$. The slope is in good agreement with the predicted value of -0.021. The intercept of the ΔE_{BC} versus log v plot in conjunction with eq 9 and values of $D = 1.3 \times 10^{-5}$ cm^2 s^{-1} and $\alpha_2 = 0.38$ establishes a second linear relationship between $\Delta E^{\circ\prime}$ and $k_{sh,2}$ for the Mo couple:

$$\log(k_{sh,2})_{Mo} = -6.53(\Delta E^{\circ\prime})_{Mo} - 0.648 \quad (10a)$$

TABLE 2: Thermodynamic and Kinetic Parameters for the $[Mo_2(\mu\text{-}PPh_2)_2(CO)_8]^{0/2-}$ and $[W_2(\mu\text{-}PPh_2)_2(CO)_8]^{0/2-}$ Couples[a]

	$[Mo_2(\mu\text{-}PPh_2)_2(CO)_8]^{0/2-}$	$[W_2(\mu\text{-}PPh_2)_2(CO)_8]^{0/2-}$
$E_1^{\circ\prime}$ (V)	−1.01 (1)	−1.00 (2)
$k_{sh,1}$ (cm s^{-1})	0.4 (1)	0.8 (5)
α_1	0.50	0.50
$E_2^{\circ\prime}$ (V)	−0.84 (1)	−0.82 (2)
$k_{sh,2}$ (cm s^{-1})	0.038 (6)	0.014 (2)
α_2	0.38	0.43
$\Delta E^{\circ\prime}$ (mV)[b]	+170	+180
$E^{\circ\prime}_{obs}$ (V)[c]	−0.925	−0.91

[a] In 0.3 M $TBAPF_6$/acetone. [b] $E_2^{\circ\prime} - E_1^{\circ\prime}$. [c] $(E_1^{\circ\prime} + E_2^{\circ\prime})/2$.

For $\mathbf{2}^{0/2-}$, the experimental relationship is $\Delta E_{BC} = -0.011 \log v + 0.0071$, which in conjunction with eq 6, $D = 1.3 \times 10^{-5}$ cm^2 s^{-1}, and $\alpha_2 = 0.43$ yields the second linear equation for the W couple:

$$\log(k_{sh,2})_W = -7.31(\Delta E^{\circ\prime})_W - 1.23 \quad (10b)$$

Simultaneous solution of eqs 8a and 10a yields $(\Delta E^{\circ\prime})_{Mo} = 0.161$ V and $(k_{sh,2})_{Mo} = 2.0 \times 10^{-2}$ cm s^{-1}. Simultaneous solution of eqs 8b and 10b yields $(\Delta E^{\circ\prime})_W = 0.149$ V and $(k_{sh,2})_W = 4.9 \times 10^{-3}$ cm s^{-1}. Recognition that $\Delta E^{\circ\prime} = E_2^{\circ\prime} - E_1^{\circ\prime}$ and $E^{\circ\prime}_{obs} = (E_1^{\circ\prime} + E_2^{\circ\prime})/2$ leads to the following initial estimates of the kinetic and thermodynamic parameters for $\mathbf{1}^{0/2-}$ and $\mathbf{2}^{0/2-}$. For the Mo couple: $E_1^{\circ\prime} = -0.998$ V, $k_{sh,1} = 1.0$ cm s^{-1}, $\alpha_1 = 0.50$, $E_2^{\circ\prime} = -0.837$ V, $k_{sh,2} = 2.0 \times 10^{-2}$ cm s^{-1}, $\alpha_2 = 0.50$; for the W couple: $E_1^{\circ\prime} = -0.954$ V, $k_{sh,1} = 1.0$ cm s^{-1}, $\alpha_1 = 0.50$, $E_2^{\circ\prime} = -0.805$ V, $k_{sh,2} = 4.9 \times 10^{-2}$ cm s^{-1}, $\alpha_2 = 0.43$.

Digital Simulations. The values of $E_1^{\circ\prime}$, $k_{sh,1}$, α_1, $E_2^{\circ\prime}$, $k_{sh,2}$, and α_2 determined above and experimental values of $R_u = 168$ Ω, $C_{dl} = 6.2 \times 10^{-8}$ F, $D = 1.3 \times 10^{-5}$ cm^2 s^{-1}, Hg drop mass = 1.63 mg, and $C = 0.1-0.3$ mM are used as input parameters for digital simulations. Simulated voltammograms are fit to experimental curves at four sweep rates between 10 and 100 V s^{-1} as described in the Experimental Section. Numerical results are presented in Table 2. The uncertainties correspond to a variation of ±10 mV in simulated values of ΔE_p at $v = 100$ V s^{-1}. Figure 3 shows the agreement between simulated and experimental traces at two sweep rates for $\mathbf{1}^{0/2-}$. The agreement between simulated and observed peak potentials over the scan-rate range $v = 0.1-100$ V s^{-1} is illustrated in Figure 2.

The results in Table 2 reveal several aspects regarding the one-electron reactions of $\mathbf{1}^{0/2-}$ and $\mathbf{2}^{0/2-}$. The thermodynamics of eqs 1 and 2 are highly inverted. Values $\Delta E^{\circ\prime} = +170$ and +180 mV are obtained for $\mathbf{1}^{0/2-}$ and $\mathbf{2}^{0/2-}$, respectively, indicating that the second charge transfer is thermodynamically more favorable than the first. However, the second electron-transfer reaction exhibits slower kinetics. The value of $k_{sh,2}$ is 10 times smaller than $k_{sh,1}$ for M = Mo and 60 times smaller than $k_{sh,1}$ for M = W. The thermodynamic and kinetic parameters of the one-electron electrode reactions are metal-dependent only to a small extent. Values of $E_1^{\circ\prime}$ and $E_2^{\circ\prime}$ are 0.01−0.02 V more positive for M = W than for M = Mo, and $(k_{sh,2})_W$ is ∼3 times smaller than $(k_{sh,2})_{Mo}$.

Disproportionation. A further consideration in multielectron reactions is the extent to which disproportionation (eq 11) participates in the electrode reaction mechanism.

$$2\,[M_2(\mu\text{-}PPh_2)_2(CO)_8]^{\bullet -} \rightleftharpoons [M_2(\mu\text{-}PPh_2)_2(CO)_8]^0 + [M_2(\mu\text{-}PPh_2)_2(CO)_8]^{2-} \quad K_{disp} \quad (11)$$

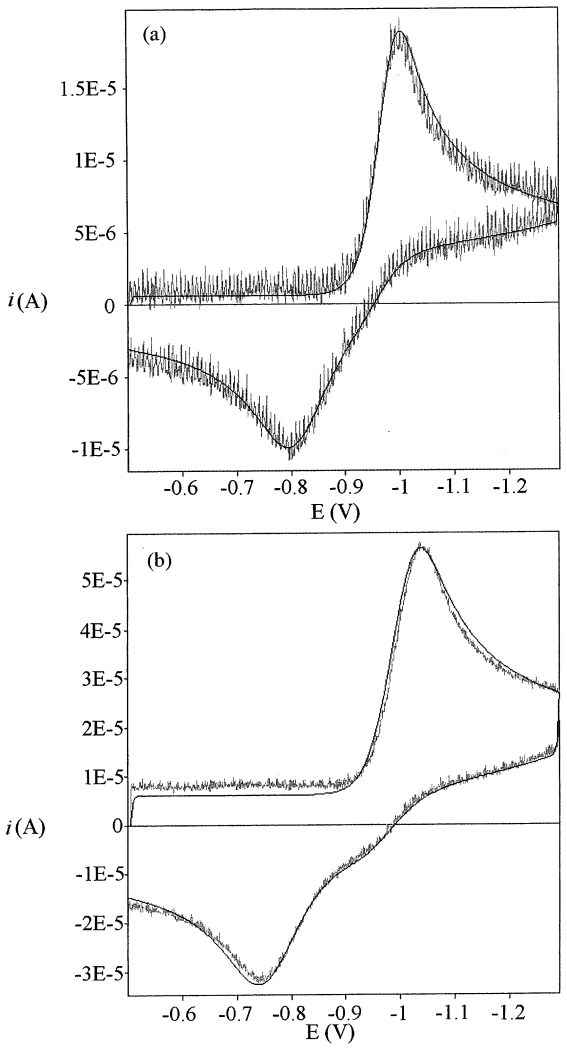

Figure 3. Fits of experimental and simulated cyclic voltammograms for $\mathbf{1}^{0/2-}$ at (a) $\upsilon = 10$ V s^{-1} and (b) $\upsilon = 100$ V s^{-1}.

Reaction 11 is thermodynamically favored because $K_{disp} = k_{f,disp}/k_{b,disp} = \exp[F(E_2^{\circ\prime} - E_1^{\circ\prime})/RT = 1 \times 10^3$. However, we conclude that disproportionation does not contribute to the experimental response for the $[M_2(\mu\text{-}PPh_2)_2(CO)_8]^{0/2-}$ systems. Voltammetric experiments conducted at concentrations of 0.1−0.3 mM do not exhibit a dependence on concentration, and simulations conducted with $C = 0.1-10$ mM, $\upsilon = 1-1000$ V s^{-1}, and $k_{f,disp} = 10^4-10^8$ M^{-1} s^{-1} using the electrode kinetic parameters in Table 2 exhibit no contribution from eq 11.

Discussion

EHMO Calculations. The electrochemical reduction of **1**° and **2**° to $\mathbf{1}^{2-}$ and $\mathbf{2}^{2-}$, respectively, occurs by concerted electron transfer and metal−metal bond cleavage. The redox active orbital is the b_{3u} σ* orbital that arises from antibonding interaction between the d_{x2-y2} orbitals of the two metals. This orbital is the vacant LUMO in the $M(I)_2$ oxidation level and the filled HOMO in the $M(0)_2$ level (Figure 4). The orbital exhibits significant metal d_{x2-y2} (22%) plus phosphorus p_x (12%) character in the $M(I)_2$ state. The metal content increases to 36% and the phosphorus content decreases to 8% in the $M(0)_2$ state. The remaining σ, π, and δ orbitals in the metal−metal bonding manifold are largely metal−carbonyl in character. They contain little or no contributions from the bridging ligands, and their compositions are not influenced by the change in oxidation state.

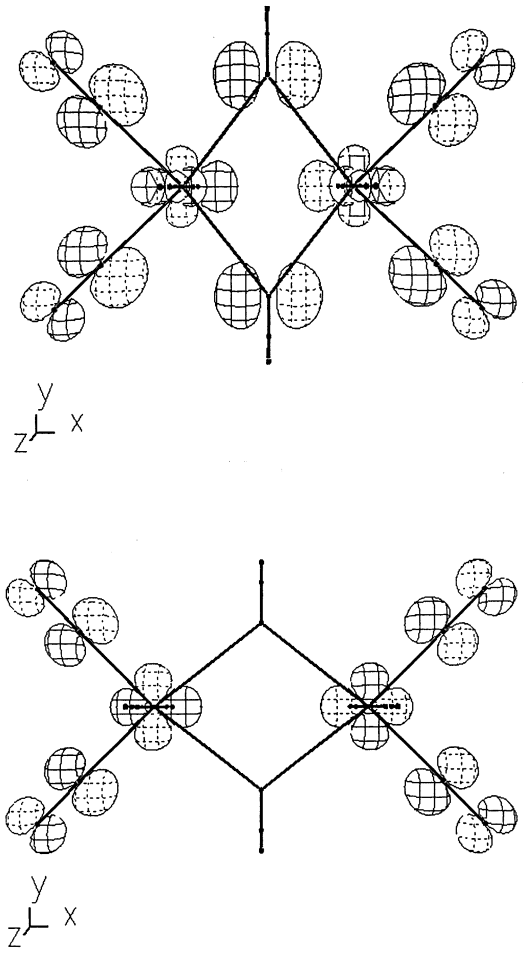

Figure 4. CACAO drawings of the σ* orbital in **2**° (top) and $\mathbf{2}^{2-}$ (bottom).

Filling of the σ* orbital cancels the metal−metal bond in the molecule.

A Walsh diagram obtained from EHMO calculations on the H_2P^- analogue of the $\mathbf{2}^{0/2-}$ couple is presented in Figure 5. The significant feature of the diagram is the dependence of the σ* orbital energy on the M−P−M bridge angle. The energy of this orbital decreases markedly on passing from the neutral **1**° and **2**° forms, where θ(M−P−M) ≈ 75°, to the $\mathbf{1}^{2-}$ and $\mathbf{2}^{2-}$ dianions, where θ(M−P−M) ≈ 104°. The energies of the other metal-based orbitals remain relatively unchanged. The result in Figure 5 supports the interpretation that metal−metal bond cleavage and its accompanying nuclear reorganization are major contributors to the driving force for coincident two-electron transfer. Solvation and ion-pair formation also may be factors in this process.[22] The Walsh diagram suggests that, as an electron is added to the σ* orbital of **1**° or **2**°, weakening of the M−M bond causes the metals to move apart and the M−P−M bond angle to increase. These nuclear displacements produce a decrease in the σ* orbital energy, which enables a second electron to be added at a potential equal to or lower than the first, resulting in a multielectron event.

Electrochemical Parameters. The electrochemical results confirm the near-coincident nature of the $\mathbf{1}^{0/2-}$ and $\mathbf{2}^{0/2-}$ conversions and provide insight into the extent to which the energetics associated with structural change are partitioned between the individual steps of the electrode reaction. The large potential inversion ($\Delta E^{\circ\prime} \cong 0.18$ V) indicates that significant thermodynamic stabilization occurs in the second step of the $\mathbf{1}^{0/2-}$ and $\mathbf{2}^{0/2-}$ reductions. However, addition of the second

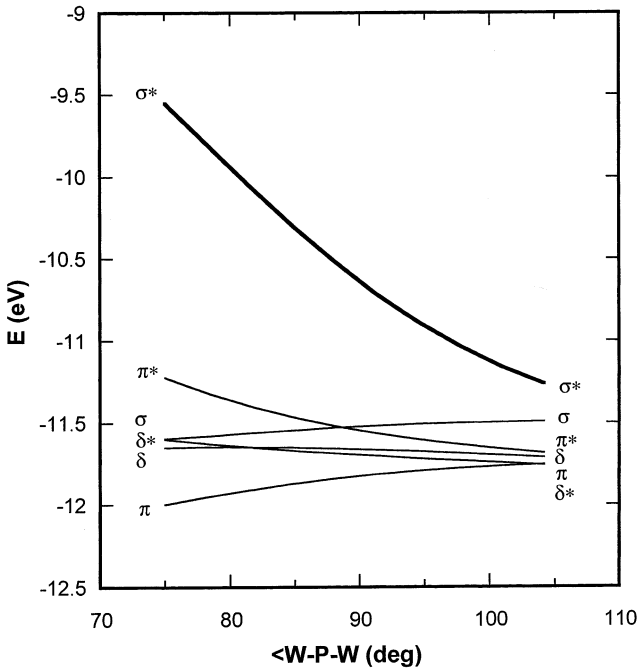

Figure 5. Walsh diagram from EHMO calculations on the H_2P^- analogue of $\mathbf{2}^{0/2-}$.

electron is rate-limiting for both couples. The latter fact is indicated by the relative breadths of the anodic versus cathodic peaks (Figure 1b) and is confirmed by digital simulations, which produce small values of $k_{sh,2}$ in comparison with $k_{sh,1}$. The rate constant ratios, $k_{sh,2}/k_{sh,1}$, correspond to a difference of 6−10 kJ mol^{-1} in free energy of activation at 298 K. Because outer-shell reorganization energies are the same for 0/1− and 1−/2− electrode reactions,[43,44] it is concluded that inner-shell reorganization is responsible for the smaller values of $k_{sh,2}$. Thus, we conclude that *the major fraction of structural change accompanying the two-electron reduction of* $\mathbf{1}^0$ *and* $\mathbf{2}^0$ *occurs in the second step of the reaction.*

It is of interest to compare results for the $[M_2(\mu\text{-}PPh_2)_2(CO)_8]^{0/2-}$ couples with those of other two-electron reactions characterized by large structural change. The behavior of $\mathbf{1}^{0/2-}$ and $\mathbf{2}^{0/2-}$ is closely paralleled by that of the arsenido-bridged complex, *cis*-$[Ru_2(\mu\text{-}AsPh_2)_2(Cp)_2(CO)_2]^{2+}$ ($\mathbf{4}^{2+}$), which undergoes two-electron reduction accompanied by cleavage of a Ru−Ru single bond.[15,45] For $\mathbf{4}^{2+/0}$, $\Delta E^{\circ\prime} = +180$ mV, $k_{sh,1} > 0.1$ cm s^{-1}, and $k_{sh,2} = 7 \times 10^{-3}$ cm s^{-1}. Thus, in these three examples of concerted two-electron transfer and metal−metal bond breaking, potential inversion is large and the rate-limiting reaction is the second step in the reduction, which completes cleavage of the metal−metal single bond.

It also is of interest to compare results with those found for the two-electron reduction of $[(\eta^6\text{-}C_6Me_6)_2Ru]^{2+}$ to $[(\eta^4\text{-}C_6Me_6)(\eta^6\text{-}C_6Me_6)Ru]^0$ ($\mathbf{5}^{2+/0}$),[46] wherein the structural change is a decrease in hapticity of one hexamethylbenzene ring. For $\mathbf{5}^{2+/0}$, $\Delta E^{\circ\prime} = +30$ mV, $k_{sh,1} \geq 2$ cm s^{-1}, and $k_{sh,2} = 4.5 \times 10^{-4}$ cm s^{-1} in CH_3CN. Although these parameters are qualitatively similar to those of $\mathbf{1}^{0/2-}$, $\mathbf{2}^{0/2-}$, and $\mathbf{4}^{2+/0}$, the individual steps of the $\mathbf{5}^{2+/0}$ reaction can be resolved at large-scan rates and disproportionation (eq 11) is observed. Thus, small quantitative differences in $\Delta E^{\circ\prime}$ and individual k_{sh} values can lead to large qualitative differences in experimental response and behavior. Further detailed study of inverted two-electron-transfer reactions would be of interest in this regard.

Influence of Metal and Bridging Ligand. It is anticipated that the identity of the metal atom and bridging ligand will influence values of $E^{\circ\prime}$ and k_{sh}. One expectation is that it is more difficult to reduce the heavier elements within the same group of the periodic table. For example, in high oxidation state oxo compounds of Mo and W, where the added electron is localized in a metal-centered orbital, $\delta E^{\circ\prime} = E^{\circ\prime}_{Mo} - E^{\circ\prime}_{W} \cong 0.6$ V.[47,48] In M−Fe−S clusters, where the redox orbital is delocalized over sulfur-bridged metal centers, $\delta E^{\circ\prime} = 0.0$−0.2 V.[49−51] For $\mathbf{1}^{0/2-}$, $\mathbf{2}^{0/2-}$, and the corresponding RS^- bridged couples (Table 1), values of $E^{\circ\prime}_1$, $E^{\circ\prime}_2$, and $E^{\circ\prime}_{obs}$ are effectively metal-independent. This observation is attributed to the π-acid character of the CO ligands, which is effective in distributing charge over the entire molecule, and to the fact that the vacant σ^* orbital in $\mathbf{1}^\circ$ and $\mathbf{2}^\circ$ is delocalized over the four-atom M_2P_2 center by mixing of metal $d_{x^2-y^2}$ and phosphorus p_x orbitals. The significant bridging-ligand contribution to the σ^* redox orbital is consistent with the large difference (∼0.5 V) in $E^{\circ\prime}$ values between Ph_2P^- and PhS^- bridged complexes. Thus, the bridging ligand exerts a greater influence than the metal on the thermodynamics of the electron-transfer reactions.

Both the metal atom and bridging ligand influence the kinetics of electron transfer. The expectation in this regard is that bonds involving W are stronger than those involving Mo,[52] which should lead to larger inner-shell reorganization energies and slower rates of electron transfer for tungsten-containing species. The rate ratio $(k_{sh,2})_{Mo}/(k_{sh,2})_W = 2.7$ is consistent with this expectation, but its value is smaller than anticipated. Previous interpretations of concerted electron transfer and metal−metal bond cleavage[10,15] have utilized the dissociative electron-transfer model of Saveant,[53] wherein the inner-shell contribution to the free energy of activation is equated to one-fourth of the bond dissociation energy. The Mo−Mo and W−W single bond energies in $\mathbf{1}^\circ$ and $\mathbf{2}^\circ$ are calculated to equal 74 and 98 kJ mol^{-1}, respectively, from the equation of Hughes and Wade[54] using metal−metal distances of d(Mo−Mo) = 3.022 Å[33] and d(W−W) = 3.026 Å.[31] From these data, it is predicted that $(k_{sh,2})_{Mo}/(k_{sh,2})_W = 11.2$, which is larger than the value observed. This result suggests that inner-shell reorganization is distributed to some extent between the two charge-transfer steps and that factors in addition to metal−metal bond energies influence inner-shell reorganization barriers.

The bridging ligand exerts a larger influence than does the metal on the kinetics of the second electron-transfer reaction. Previously, we estimated $k_{sh,2} \cong 0.1$ cm s^{-1} for the second step of the $[W_2(\mu\text{-}SBz)_2(CO)_8]^{0/2-}$ reaction.[10] Although the bridging-ligand substituent groups differ, comparison to the data for $\mathbf{2}^{0/2-}$ in Table 2 indicates that electron transfer is faster for sulfido-bridged than for phosphido-bridged species. The origin of this difference is unclear. Examination of X-ray structural data for $[W_2(\mu\text{-}SPh)_2(CO)_8]$,[55] $[Et_4N]_2[W_2(\mu\text{-}SPh)_2(CO)_8]$,[56] $[W_2(\mu\text{-}PPh_2)_2(CO)_8]$,[31] and $[Li(THF)_3]_2[W_2(\mu\text{-}PPh_2)_2(CO)_8]$[31] reveals that metrical changes within the four-atom, ligand-bridged unit resulting from two-electron transfer are almost identical for $W_2(\mu\text{-}SPh)_2$ and $W_2(\mu\text{-}PPh_2)_2$ complexes.[57] It is possible that differences in metal−ligand force constants for W−S versus W−P bond-length and bond-angle deformations could account for the difference in rates through their impact on inner-shell reorganization energies. Empirically, electron-transfer kinetics often parallel thermodynamic trends, with stronger metal−ligand interactions correlating with more difficult reduction and a slower rate of reaction.[58,59] On this basis, slower electron transfer is anticipated for $W_2(\mu\text{-}PPh_2)_2$ versus $W_2(\mu\text{-}SPh)_2$ species given the 0.5 V difference in electrode potentials. However, the bond-distance/force-constant equations of Woodruff et al.[60] predict identical values for W−S and W−P bond deformation constants

on the basis of the structural information cited above. Spectroscopic data and normal coordinate analyses of vibrations within the four-atom W_2S_2 and W_2P_2 cores would be helpful in understanding the differences exhibited by these systems. It is evident that the bridging ligand plays an important role in controlling the kinetics and thermodynamics of concerted two-electron transfer and metal−metal bond cleavage.

Conclusion

The phosphido-bridged Mo(I) and W(I) carbonyl dimers, $[M_2(\mu\text{-}PPh_2)_2(CO)_8]^0$ (M = Mo, W), undergo concerted two-electron transfer accompanied by metal−metal bond cleavage upon reduction to their corresponding dianions. Large electron-transfer-induced structural changes within the four-atom $M_2(\mu\text{-}PPh_2)_2$ unit lead to an inversion of one-electron redox potentials. Although addition of the second electron, which completes the cleavage of the metal−metal bond, is rate-limiting, inner-shell reorganization is divided to some extent between the two charge-transfer steps. EHMO calculations reveal that the redox-active orbital is a metal−metal antibonding (σ^*) orbital with substantial bridging-ligand character that decreases markedly in energy on passing from the metal−metal bonded $M(I)_2$ state to nonbonded $M(0)_2$. The thermodynamics and kinetics of the one-electron electrode reactions exhibit a small dependence on metal but are influenced to a greater extent by the identity (R_2P^- or RS^-) of the bridging ligand.

Acknowledgment. The authors gratefully acknowledge support from the National Science Foundation, the American Chemical Society Petroleum Research Fund, and the Purdue Research Foundation.

References and Notes

(1) Collman, J. P.; Wagenknecht, P. S.; Hutchinson, J. E. *Angew. Chem., Int. Ed. Engl.* **1994**, *33*, 1537.
(2) Zusman, L. D.; Beratan, D. N. *J. Phys. Chem. A* **1997**, *101*, 4136.
(3) Evans, D. H.; Lehmann, M. W. *Acta Chem. Scand.* **1999**, *53*, 765.
(4) Koppenhöfer, A.; Turner, K. L.; Allen, J. W. A.; Chapman, S. K.; Ferguson, S. J. *Biochemistry* **2000**, *39*, 4243.
(5) Ram, M. S.; Skeens-Jones, L. M.; Johnson, C. S.; Zhang, X. L.; Stern, C.; Yoon, D. I.; Selmarten, D.; Hupp, J. T. *J. Am. Chem. Soc.* **1995**, *117*, 1411.
(6) Stoll, M. E.; Belanzoni, P.; Calhorda, M. J.; Drew, M. G. B.; Félix, V.; Geiger, W. E.; Gamelas, C. A.; Gonçalves, I. S.; Ramão, C. C.; Veiros, L. F. *J. Am. Chem. Soc.* **2001**, *123*, 10595.
(7) Savéant, J.-M. *J. Phys. Chem. B* **2001**, *105*, 8995.
(8) Zhuang, B.; McDonald, J. W.; Schultz, F. A.; Newton, W. E. *Organometallics* **1984**, *3*, 943.
(9) Smith, D. A.; Zhuang, B.; Newton, W. E.; McDonald, J. W.; Schultz, F. A. *Inorg. Chem.* **1987**, *26*, 2524.
(10) Fernandes, J. B.; Zhang, L. Q.; Schultz, F. A. *J. Electroanal. Chem.* **1991**, *297*, 145.
(11) Hill, M. G.; Rosenhein, L. D.; Mann, K. D.; Mu, X. H.; Schultz, F. A. *Inorg. Chem.* **1992**, *31*, 4108.
(12) Collman, J. P.; Rothrock, R. K.; Finke, R. G.; Moore, E. J.; Rose-Munch, F. *Inorg. Chem.* **1982**, *21*, 146.
(13) Koide, Y.; Bautista, M. T.; White, P. S.; Schauer, C. K. *Inorg. Chem.* **1992**, *31*, 3690.
(14) Collins, B. E.; Koide, Y.; Schauer, C. K.; White, P. S. *Inorg. Chem.* **1997**, *36*, 6172.
(15) DiMaio, A.-J.; Rheingold, A. L.; Chin, T. T.; Pierce, D. T.; Geiger, W. E. *Organometallics* **1998**, *17*, 1169.
(16) Teo, B. K.; Hall, M. B.; Fenske, R. F.; Dahl, L. F. *J. Organomet. Chem.* **1974**, *70*, 413.
(17) Teo, B. K.; Hall, M. B.; Fenske, R. F.; Dahl, L. F. *Inorg. Chem.* **1975**, *14*, 3103.
(18) Burdett, J. K. *J. Chem. Soc., Dalton Trans.* **1977**, 423.
(19) Shaik, S.; Hoffmann, R.; Fisel, C. R.; Summerville, R. H. *J. Am. Chem. Soc.* **1980**, *102*, 4555.
(20) Rizzi, G. A.; Granozzi, G.; Casarin, M.; Basato, M. *Organometallics* **1987**, *6*, 2536.
(21) Reinhold: J.; Müller, B.; Eichler, U. *Organometallics* **1997**, *16*, 1497.
(22) Baik, M.-H.; Ziegler, T.; Schauer, C. K. *J. Am. Chem. Soc.* **2000**, *122*, 9143.
(23) (a) Howard, J. B.; Rees, D. C. *Chem. Rev.* **1996**, *96*, 2965. (b) Burgess, B. K.; Lowe, D. J. *Chem. Rev.* **1996**, *96*, 2983.
(24) (a) Chan, M. K.; Kim, J. S.; Rees, D. C. *Science*, **1993**, *260*, 792. (b) Mayer, S. M.; Lawson, D. M.; Gormal, C. A.; Row: S. M.; Smith, B. E. *J. Mol. Biol.* **1999**, *292*, 871.
(25) (a) Rees, D. C.; Chan, M. K.; Kim, J. *Adv. Inorg. Chem.* **1994**, *40*, 89. (b) Rees, D. C.; Howard, J. B. *Curr. Opin. Chem. Biol.* **2000**, *4*, 559.
(26) Han, J.; Beck, K.; Ockwig, N.; Coucouvanis, D. *J. Am. Chem. Soc.* **1999**, *121*, 10448.
(27) Coucouvanis, D.; Han, J.: Moon, N. *J. Am. Chem. Soc.* **2002**, *124*, 216.
(28) Ibrahim, S. K.; Vincent, K.; Gormal, C. A.; Smith, B. E.; Best, S. P.; Pickett, C. J. *Chem. Commun.* **1999**, 1019.
(29) (a) Peters, J. W.; Stowell, M. H. B.; Soltis, M.; Finnegan, M. G.; Johnson, M. K.; Rees, D. C. *Biochemistry* **1997**, *36*, 1181. (b) Musgrave, K. B.; Liu, H. I.; Ma, L.; Burgess, B. K.; Watt, G.; Hedman, B.; Hodgson, K. O. *J. Biol. Inorg. Chem.* **1998**, *3*, 344.
(30) Nyborg. A. C.; Johnson, J. L.; Gunn, A.; Watt, G. D. *J. Biol. Chem.* **2000**, *275*, 39307.
(31) Shyu, S.-G.; Calligaris, M.; Nardin, G.; Wojcicki, A. *J. Am. Chem. Soc.* **1987**, *109*, 3617.
(32) Wong, W.-T.; Wong, W.-K. *Acta Crystallogr.* **1994**, *C50*, 1404.
(33) Maitra, K.; Catalano, V. J.; Nelson, J. H. *J. Organomet. Chem.* **1997**, *529*, 409.
(34) Evans, D. H.; Hu, K. *J. Chem. Soc., Faraday Trans.* **1996**, *92*, 3983.
(35) Evans, D. H. *Acta Chem. Scand.* **1998**, *52*, 194.
(36) Grim, S. O.; Wheatland, D. A.; McFarlane, W. *J. Am. Chem. Soc.* **1967**, *89*, 5573.
(37) Howell, J. O.; Kuhr, W. G.; Ensman, R. E.; Wightman, R. M. *J. Electroanal. Chem.* **1986**, *209*, 77.
(38) Roe, D. K. In *Laboratory Techniques in Electroanalytical Chemistry*; Kissinger, P. T., Heineman, W. R., Eds.; Marcel Dekker: New York, 1996; Chapter 7.
(39) Rudolph, M.; Reddy, D. R.; Feldberg, S. *Anal. Chem.* **1994**, *66*, 589A.
(40) Mealli, C.; Proserpio, D. M. *J. Chem. Educ.* **1990**, *67*, 399. The program was obtained from ftp://cacao.issecc.fi.cnr.it (accessed September 1996).
(41) (a) Ryan, M. D. *J. Electrochem. Soc.* **1978**, *125*, 547. (b) See also: Hinkelmann, K.; Heinze, J. *Ber. Bunsen-Ges. Phys. Chem.* **1987**, *91*, 243.
(42) Equation 41 in ref 41a contains an error. The correct denominator of the first term on the rhs of the equation is $(1 - \alpha_2^2)$.
(43) Marcus, R. A. *J. Chem. Phys.* **1965**, *43*, 679.
(44) Weaver, M. J. In *Comprehensive Chemical Kinetics*; Compton, R. G., Ed.; Elsevier: Amsterdam, 1987; Vol. 27, pp 1−60.
(45) Studies of $\mathbf{4}^{2+/0}$ in ref 15 were conducted by oxidizing **4**°. However, the couple is represented here as a reduction to correlate its electron-transfer-induced metal−metal bond cleavage with that of $\mathbf{1}^{0/2-}$ and $\mathbf{2}^{0/2-}$.
(46) Pierce, D. T.; Geiger, W. E. *J. Am. Chem. Soc.* **1992**, *114*, 6063.
(47) Charney, L. M.; Schultz, F. A. *Inorg. Chem.* **1980**, *19*, 1527.
(48) Bradbury, J. R.; Schultz, F. A. *Inorg. Chem.* **1986**, *25*, 4408.
(49) Christou, G.; Garner, C. D.; Miller, R. N.; Johnson, C. E.; Rush, J. D. *J. Chem. Soc., Dalton Trans.* **1980**, 2363.
(50) Armstrong, W. H.; Mascharak, P. K.; Holm, R. H. *J. Am. Chem. Soc.* **1982**, *104*, 4373.
(51) Zanello, P. *Coord. Chem. Rev.* **1988**, *87*, 1.
(52) Bauer, A.; Capps, K. B.; Wixmerten, B.; Abboud, K. A.; Hoff, C. D. *Inorg. Chem.* **1999**, *38*, 2136.
(53) Savéant, J.-M. *J. Am. Chem. Soc.* **1987**, *107*, 6788.
(54) $E(M-M) = A \cdot d(M-M)^{-4.6}$, where $d(M-M)$ is the metal−metal bond distance in pm and $A = 1.888 \times 10^{13}$ for Mo and 2.519×10^{13} for W: Hughes, A. K.; Wade, K. *Coord. Chem. Rev.* **2000**, *197*, 191.
(55) Zhuang, B.; Sun, H.; Pan, G.; He, L.; Wei, Q.; Zhou, Z.; Peng, S.; Wu, K. *J. Organomet. Chem.* **2001**, *640*, 127.
(56) Darensbourg, D. J.; Sanchez, K. M.; Reibenspies, J. *Inorg. Chem.* **1988**, *27*, 3636.
(57) The electron-transfer-induced structural differences are $\Delta d(W-W) = 1.09$ Å, $\Delta d(W-S) = 0.11$ Å, $\Delta\theta(W-S-W) = \Delta\theta(S-W-S') = 29°$ for $[W_2(\mu\text{-}SPh)_2(CO)_8]^{0/2-}$, and $\Delta d(W-W) = 1.08$ Å, $\Delta d(W-P) = 0.12$ Å, $\Delta\theta(W-P-W) = \Delta\theta(P-W-P') = 29°$ for $[W_2(\mu\text{-}PPh_2)_2(CO)_8]^{0/2-}$.
(58) Faure, D.; Lexa, D.; Savéant, J.-M. *J. Electroanal. Chem.* **1982**, *140*, 297.
(59) Lexa, D.; Savéant, J.-M. *Acc. Chem. Res.* **1983**, *16*, 235.
(60) Conradson, S. D.; Sattelberger, A. P.; Woodruff, W. H. *J. Am. Chem. Soc.* **1988**, *110*, 1309.